Boundary-Layer Meteorol (2012) 142:443–467
DOI 10.1007/s10546-011-9681-6

ARTICLE

Effects of Wall Heating on Flow Characteristics in a Street Canyon

Xiao-Ming Cai

Received: 29 December 2010 / Accepted: 19 November 2011 / Published online: 7 December 2011

Abstract We develop a large-eddy simulation (LES) model based on a meteorological numerical model for a real scale street-canyon flow with rough building facets heated by a given temperature. The model is applied to a canyon with the aspect ratio of unity for two idealized heating scenarios: (1) the roof and the entire upstream wall are heated, named as 'assisting cases', and (2) the roof and the entire downstream wall are heated, named as 'opposing cases'. These facets were heated up to 15 K above the air temperature. A wall function for temperature is proposed for a rough facet with an assumption that the thermal roughness length, z_{0T}, is much smaller than the aerodynamic roughness length, z_0. It is demonstrated that the sensible heat flux and canyon-air temperature are significantly influenced by the near-facet process that is parametrized by z_{0T} as the primary factor; other processes such as in-canyon mixing and roof-level exchange are secondary. This new finding strongly suggests that it is vital to choose an appropriate value of z_{0T} in a numerical simulation of street-canyon flows with the facet-air exchange processes of heat or any scalar. The finding also raises an awareness of the demand for carefully designed laboratory or field experiments of quantifying z_{0T} values for various urban surfaces. For the opposing cases, an unsteady penetrating narrow updraft zone appears occasionally along the heated wall and this feature is consistent field observations. The unique result indicates the superior capability of LES. The results of this study can be used to guide the parametrization of turbulent processes inside the urban canopy layer.

Keywords Large-eddy simulation · Solar radiation · Turbulent characteristics · Urban street canyon · Wall heating

X.-M. Cai (✉)
School of Geography, Earth and Environmental Sciences, University of Birmingham, Edgbaston, Birmingham, B15 2TT, UK
e-mail: x.cai@bham.ac.uk

1 Introduction

From a geometric perspective an urban surface is characterized by repeating units consisting of a road lined on either side by opposing buildings. The climatic conditions inside these 'street canyons' are largely influenced by the conditions in the urban boundary layer (UBL) and turbulent exchange of momentum and heat with the underlying canyons (namely the urban canopy layer). The exchange between the UBL and the urban canopy layer under neutral conditions (i.e. the surface temperatures at the street, the wall, and the roof are the same as the air temperature) has been examined using wind-tunnel experiments (Barlow et al. 2004; Narita 2007) and numerical modelling (Baik and Kim 1999; Kim and Baik 2004; Liu and Barth 2002; Liu et al. 2004, 2005).

However, a street canyon in reality is subject to solar heating, which enhances the turbulent exchange significantly (Louka et al. 2002), but quantification of the enhancement is extremely challenging due to the involvement of various complicated processes. First of all, as the major energy input, the total solar radiation energy flux entering the urban canopy layer during the day depends on the latitude of the city and the characteristics of the built form (e.g. orientation of the streets and the density of building blocks) (Oleson et al. 2008). Secondly the physical parameters of building materials affect the heat energy stored in the buildings as well as the surface temperature of the building surfaces. These parameters include albedo (determining the absorbed amount of solar radiation), heat conductivity (influencing heat transfer rate into the building materials), and heat capacity (linking heat to temperature), and these parameters vary from city to city (Salamanca et al. 2010). Finally the surface temperature of building surfaces is determined by the energy balance between the received net radiation, the heat storage into the building materials through heat conduction, and the sensible and latent heat fluxes transferred to the air through turbulent mixing, if anthropogenic heat source and heterogeneous advective heat divergence are negligible. Field observations showed that the energy-balance characteristics vary with latitude, urban geometry, and surface material (e.g. Grimmond and Oke 1999). This is also supported by a study in which the energy-balance characteristics are compared between an Asian city and a European city (Kawai and Kanda 2010). Among all components in the energy balance mentioned above, the most challenging task is to quantify the sensible and latent heat fluxes transferred to the air through the turbulent mixing for a given temperature at the building surfaces. This has been indicated by very scattered data of sensible and latent heat fluxes from observations (e.g. Kawai and Kanda 2010). The underlying processes controlling the fluxes are the turbulent flows around the buildings, which can be significantly altered by the thermally driven updrafts. A good understanding of the processes is essential to the quantification of the energy balance over an urban surface. This is also valuable to the parametrization of urban canyon mechanisms to be used in a mesoscale meteorological model, a regional climate model, or an urban air quality model. However, little is known about the modifications to the turbulent mixing due to the sensible heat flux released from the canyon walls and the roads (Offerle et al. 2007).

Some field observations have been made in order to understand the effects of solar radiation on temperature and airflow in and above a street canyon. An early attempt to measure the temperature distribution in a street canyon was made in Kyoto, Japan, by Nakamura and Oke (1988), where the aspect ratio defined as H/W is about 1.06, in which H is building height and W is the canyon width. The data showed that the surface-air temperature differences are as large as 8–9 K for the sunlit wall and 12–14 K for the roof, and suggested that the thermal effects on temperature and flow are restricted to a narrow zone of the heated wall. Another field study carried out in a nearly south-to-north oriented street canyon ($H/W \approx 1.4$) in Nantes, France, in 1999 has also examined the effects of heated urban facets on the flow in a

street canyon (Louka et al. 2002). Their observations suggested that a layer of strong mean-temperature gradient near the heated wall can be as thin as 0.2 m in the canyon with $W \approx 15$ m. Unfortunately no wind measurement was made within 1.5 m from the walls; therefore the observations suggested that the thermally-driven updrafts near the walls, if existed, should be thinner than one tenth of the street width. A recent field experiment has been carried out by Offerle et al. (2007) for a deep street canyon ($H/W \approx 2$). They found that the thermal effects on the flow inside the canyon are not as large as those shown in numerical experiments (reviewed below). For a downstream-wall-heated case, the turbulent exchange is enhanced, whilst for an upstream-wall-heated case, the heat transfer is much more concentrated near the wall. The buoyancy effects on the flow pattern were not observable in their coarse arrangement of wind sensors. In another recent field study, JAPEX (Idczak et al. 2007), based on a 1:5 scaled street-canyon model with H/W =2.5, Idczak et al. (2007) found that the flow pattern inside the canyon was not significantly affected by the wall heating. The thermal layer near the heated wall was generally thin and is not observable in their settings. They suggested that thermal effects on the flow pattern are considerable only in the location very near the heated wall.

There is a lack of wind-tunnel experiments that are designed to examine the effects of wall heating on the flow structure in a street canyon. There are two reasons for this. First, it is difficult to control the heating conditions for small building elements that are normally of scale on the order of tens of mm. Second, it is difficult to satisfy the independent requirements for both Reynolds number ($Re = U_{\mathrm{ref}} H/\nu$, where ν is molecular viscosity of air and U_{ref} the reference velocity) and Richardson number ($Ri = gH(T_0 - T_{\mathrm{ref}})/(T_{\mathrm{ref}} U_{\mathrm{ref}}^2)$, where T_{ref} is the reference temperature and T_0 the temperature at the wall). The first requirement is easily met because Re is generally larger than 10^4 so that the turbulent characteristics are not sensitive to the value of Re. The second requirement is that the Richardson number of a wind-tunnel experiment must be equal to that in the field. This requirement is however very difficult to be satisfied because it requires an extremely large temperature difference between surface and air for a wind-tunnel experiment (Richards et al. 2006). Due to the above two reasons, most wind-tunnel studies of canyon-heating cases are confined to the bottom heating of a whole working section rather than the heating of an individual wall. An example of this kind is that conducted by Uehara et al. (2000) in which the urban canopy is comprised of heated building cubes. Richards et al. (2006) carried out a wind-tunnel experiment by heating a single leeside wall of a cubic building ($H = 0.19$ m). They found a rapid temperature decrease near the heated surface, suggesting that the majority of heat is transported away vertically by a thermal plume and not re-entrained into the wake via a recirculation region. The closest setting to the present numerical study is the wind-tunnel experiment with downstream-wall heating of a squared cavity of Kovar-Panskus et al. (2002). In the experiment, the magnitude of Ri is satisfactorily large and the wind measurement point closest to the heated wall was placed at one-tenth of the canyon width to the wall. The authors also suggested that a thermal-driven updraft is confined within a narrow zone near the heated wall. In addition, the spatial patterns of temperature near the wall have shown an upward shift when the surface heating increases.

Another approach to a better understanding of the problem is numerical modelling. This approach is free from the requirements of scaling and heating control although it may suffer from a poor representation of turbulence due to the deficiency of the parametrization scheme. Therefore modelling can compensate the weaknesses of field and laboratory experiments. Two major groups of numerical modelling have been employed for real-scale street-canyon flows: computational fluid dynamics (CFD) based on Reynolds-averaged Navier–Stokes equations (RANS) and large-eddy simulation (LES) based on subgrid-scale filtered Navier–Stokes equations. An early RANS modelling study (Sini et al. 1996) adopted a

two-dimensional (2D) street canyon (in fact, a 2D cavity) with $H/\mathrm{W} = 1.1$. Their results showed that when the upstream wall or the street is heated, the flow pattern is similar to that of the neutral case. When the downstream wall is heated, two contra-rotating vortices are formed with one above the other. Recent CFD studies (Xie et al. 2005, 2006) for an isolated canyon derived a similar feature of multiple vortices for the downstream-wall-heated cases. Applying the same model to the fifth canyon in an array of 1–1 street canyons, Xie et al. (2007) found that the secondary vortex near the downstream wall derived from the RANS model is much more intense and larger than that from the wind-tunnel observations in Kovar-Panskus et al. (2002).

In contrast, LES allows the development of large unsteady eddies and the momentum transfer is undergone through both the resolved scale and subgrid scale. It is therefore expected that LES is capable of resolving the features of thin updrafts near the heated walls suggested by observations, particularly when such updrafts are non-persistent and unsteady in character. Although there have been many LES studies of the airflow in a street canyon under neutral conditions (e.g. Cui et al. 2004; Liu et al. 2004, 2005), LES of the street-canyon flows with heated surfaces is scarce. A recent LES study of airflow in urban canyons by Li et al. (2010) examined the cases with ground heating and no report has been found in the literature on LES of the street-canyon flows under the influence of wall heating. This is thus the main focus of the present study.

To model the airflow in a street canyon with heated surfaces, one must use an appropriate boundary condition for temperature. There are two types of boundary conditions on the building surfaces for temperature (or any scalar): (1) a given flux at the facets (e.g. sensible heat flux at the walls), and (2) a given value at the facets (e.g. temperature at the walls). In the present study, a given value of temperature is used for the cases of heating surfaces. This type of boundary condition has more applications because temperature data can be readily acquired from direct measurements or remote sensing observations.

For a rough surface a well-established approach to the boundary condition for temperature (or any scalar) is based on the Reynolds analogy. Within this framework the knowledge of heat (or scalar) transfer near the wall is obtained from the understanding of momentum transfer. In the formulation, two roughness lengths, z_0 and $z_{0\mathrm{T}}$, are used for momentum and temperature, respectively. For a smooth surface the boundary condition for temperature is parametrized primarily through the molecular properties of air (Garratt 1992). In reality however, the majority of building surfaces are not dynamically smooth and normally consist of rough elements of bluff bodies. For a turbulent flow over a rough surface, the dependence of heat transfer on the molecular properties becomes weak. This is because the momentum flux is dominated by the form drag induced by the pressure variations around the rough elements, whereas the heat or mass transfer has no clear link to the pressure field (Garratt 1992). Observations have shown that the rougher the surface is, the less efficient heat transfer will be in comparison with momentum transfer because the form drag increases with surface roughness. In a formulation of the Reynolds analogy, this implies that $z_{0\mathrm{T}} \ll z_0$ (Brutsaert 1975, 1982). This difference must be considered because the measured $z_{0\mathrm{T}}$ can be several orders of magnitude smaller than z_0 (Garratt 1992) and its effects on the heat transfer are significant under certain conditions. Although this approach is phenomenologically derived and lacks consideration of processes, it has been widely used due to its simplicity and practical utility. We will adopt the Reynolds analogy in this study to formulate the boundary condition for temperature (or a scalar).

This article is organized as follows: Sect. 2 describes the boundary conditions adopted for temperature and velocity components on the urban facets, and Sect. 3 provides the details of the LES model configuration for different heating scenarios and the method of processing

the model output. Section 4 demonstrates the analyzed results and the comparisons with the experimental data of Kovar-Panskus et al. (2002), while Sect. 5 provides the conclusions.

2 Boundary Conditions on Rough Street and Building Surfaces

The boundary conditions for temperature and velocity components on a rough urban facet are based on the bulk Richardson number (Ri_B) approach proposed by Louis (1979). The relationship between Ri_B and z/L (where L is the Obukhov length) is described in detail in Garratt (1992). However, adapting Louis's scheme to a case in which $z_{0T} \neq z_0$ will inevitably involve iteration. In fact, in Uno et al. (1995), a method was proposed to reduce the computing effort. Therefore the scheme of Uno et al. (1995) is adopted in the present study as the wall-function for temperature and velocity components on an urban facet:

$$\begin{aligned} F_0^{(\varphi)} &= -\frac{\kappa^2}{\ln(z_1/z_0)\ln\left(z_1/z_{0\varphi}\right)} G_\varphi\left(z_1/z_0, z_1/z_{0\varphi}, Ri_{B1}\right)|V_1|(\varphi_1-\varphi_0) \\ &= -C_\varphi |V_1| \Delta\varphi_{1\text{-}0}, \end{aligned} \tag{1}$$

in which φ can be either V (tangential velocity component) or a scalar, for example, T (temperature), $F_0^{(\varphi)}$ is the total flux of φ at the wall (a positive value represents a flux from the wall to the air), κ is the von Karman constant, z_1 is the distance of the centre of the first cell away from the wall (= 0.15 m in this study), z_0 and $z_{0\varphi}$ are the roughness lengths of the building material for momentum and for φ (specifically, $z_{0V} = z_0$), respectively, V_1 and φ_1 are the tangential wind speed and the value of φ at z_1, respectively, φ_0 is the value of φ at the wall (theoretically the temperature at z_{0T} was assumed to equal the temperature at the wall by Uno et al. 1995), $\Delta\varphi_{1\text{-}0} = \varphi_1 - \varphi_0$, G_φ is an empirical function to be numerically derived from the method in Uno et al. (1995), Ri_{B1} is the local Richardson number defined at the first cell in the vicinity of the wall: $Ri_{B1} = gz_1\Delta T_{1\text{-}0}/(T_0 V_1^2)$, and C_φ is the exchange coefficient for φ (dimensionless).

For the neutral limit, $G_\varphi \to 1$. Thus the drag coefficient (i.e. the exchange coefficient for momentum) becomes $C_V = [\kappa/\ln(z_1/z_0)][\kappa/\ln(z_1/z_0)]$ and the exchange coefficient for temperature becomes $C_T = [\kappa/\ln(z_1/z_0)][\kappa/\ln(z_1/z_{0T})]$. The ratio of the two exchange coefficients is $C_V/C_T = \ln(z_1/z_{0T})/\ln(z_1/z_0) = 1 + \ln(z_0/z_{0T})/\ln(z_1/z_0)$. Using the conventional definition of $\kappa B_H^{-1} = \ln(z_0/z_{0T})$ and $\gamma = \kappa B_H^{-1}/\ln(z_1/z_0)$, we can write $C_V/C_T = 1 + \gamma$. Considering a rough facet for which $z_{0T} < z_0$, the value of γ is positive and thus $C_T < C_V$, i.e. the heat transfer is less efficient than the momentum transfer. From the expression of γ, we note that $C_T \approx C_V$ if $z_1 \gg z_0$ because $\gamma \to 0$ for a given value of κB_H^{-1}. For the LES in the present study ($z_1 = 0.15$m and $z_0 = 0.01$ m), however, C_T can be much smaller than C_V. For example, if $\kappa B_H^{-1} = 2$, $C_V/C_T = 1.74$; if $\kappa B_H^{-1} = 5$, $C_V/C_T = 2.85$.

Unfortunately the value of B_H^{-1} is not well documented for rough walls in reality. Several previous studies showed that the value of B_H^{-1} for a surface with bluff elements depends on the roughness Reynolds number, $Re_* = u_* z_0/\nu$. One well-known relation validated against experimental data and applicable to air is (Garratt 1992):

$$B_H^{-1} = 6.2 Re_*^{0.25} - 5 \tag{2}$$

For the present study in which $z_0 = 0.01$ m and the reference velocity, $U_{ref} = O(1)$ m s^{-1}, the roughness Reynolds number $Re_* \lesssim 100$. For example, if $Re_* = 100$, $\kappa B_H^{-1} \approx 5.8$; if $Re_* = 10$, $\kappa B_H^{-1} \approx 2.4$. In the cases of this study, $u_* \approx 0.1$ m s^{-1}, which gives the value of Re_* about 67 and the value of κB_H^{-1} about 5. Therefore, we present the LES results for

$\kappa B_{\mathrm{H}}^{-1} = 5$. In order to demonstrate the importance of the $\kappa B_{\mathrm{H}}^{-1}$ value in the wall function, the results of the cases with $\kappa B_{\mathrm{H}}^{-1} = 2$ are also presented in order to compare against those with $\kappa B_{\mathrm{H}}^{-1} = 5$ in Sect. 4.4. We know that $\kappa B_{\mathrm{H}}^{-1} = 5$ represents a rougher surface and $\kappa B_{\mathrm{H}}^{-1} = 2$ represents a smoother surface. It is noted that in the study of Cai et al. (2008) the difference between z_0 and $z_{0\mathrm{T}}$ was not considered, namely $\kappa B_{\mathrm{H}}^{-1} = 0$. They showed that this assumption is acceptable when the LES results were compared with the wind-tunnel experiments with a smooth surface.

It is noted that the scheme of Eq. 1 is widely accepted for the atmospheric surface layer over a flat surface. For a vertical wall, however, the flow is affected by both natural convection (buoyancy driven) and external wind (forced) and can thus be characterized as one of three regimes: buoyancy driven, forced, or mixed. It may be argued that for forced convection the scheme should work satisfactorily as for a horizontal surface, and for mixed convection the scheme can be taken as a good approximation.

3 Configuration of LES Model and Processing LES Results

The LES model employed in this study is developed based on the Regional Atmospheric Modeling System (RAMS). Although it was initially designed for mesoscale meteorological modelling, RAMS's dynamical core was purposely coded regardless of scales based on a set of equations for fully compressible air (Cotton et al. 2003). The advection is numerically treated by the standard second-order leapfrog scheme, and the adjustment of pressure field is based on a set of equations for fully compressible air. For a scalar (e.g. temperature), the finite-difference scheme with second-order accuracy is used to calculate the diffusion in the domain. On all building and street facets, the boundary condition, Eq. 1, is used for all relevant quantities. The dynamical part of the LES model for the neutral case with $H/W = 1$ has been validated by Cui et al. (2004), in which the mean wind and the resolved-scale turbulent kinetic energy (TKE) have been compared against wind-tunnel experiments. The scalar part of the model for the neutral case with various H/W has been validated by Cai et al. (2008), in which the normalized fluxes have been compared against wind-tunnel experiments.

In this study we adopt $H = 18$ m and $W = 18$ m; such a canyon has an aspect ratio $H/W = 1$ (see Fig. 1 for an illustration of its cross-section). The domain sizes are $L_x = 24$ m, $L_y = 40$ m, and $L_z = 90$ m. The ratio of $L_z/H = 5$ has been shown by several previous studies (Cui et al. 2004; Cai et al. 2008) to be sufficiently large if the focus is under the roof level inside the street canyon. The domain is covered by $80 \times 40 \times 91 (= 291,200)$ grid points with grid spacing of 0.3 m $\times$ 0.3 m $\times$ 1.0 m inside the canyon and the vertical grid spacing is stretched gradually above the canyon. The initial wind condition consists of zero value inside the canyon and a logarithmic profile above the roof level with $u_* = 0.23$ m s^{-1} and $z_0 = 0.9$ m. This implies a maximum wind speed $U_{\max}$ is 2.5 m s^{-1} at the top of the domain. The lateral boundary conditions for all wind components and temperature are cyclic along both the x-direction on the vertical planes passing through the middle of the two buildings (indicated by the dash-dotted lines in Fig. 1) and the y-direction at the beginning and the end of the street. This implies that the canyon is infinitely long in the y-direction and that there are an infinite number of canyons in the x-direction. The origin of the coordinate system is indicated in Fig. 1 for the purpose of matching that in Kovar-Panskus et al. (2002). The timestep for the integration is 0.03 s, which suffices for the requirement of the Courant–Friedrichs–Lewy (CFL) condition. The overall time for one-hour simulation takes about 136 CPU hours.

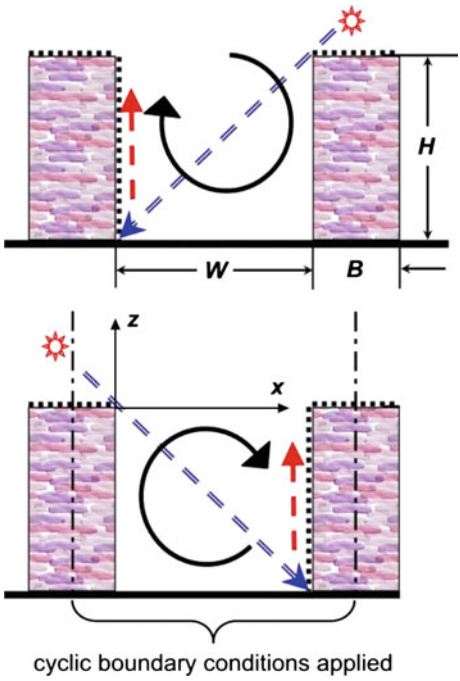

Fig. 1 Schematic diagram of the configuration of the canyon heating: **a** building roof and the upstream wall are heated by solar radiation indicated by *dashed double arrow lines*; **b** building roof and the downstream wall are heated. Background flow from *left* to *right*. *Solid dashed arrow lines* indicate the updrafts induced by the wall heating; *solid arrow curves* indicate the primary vortex driven by the background wind. Building height and width are H and B, respectively and street width is W. The *dash-dotted lines* indicate the domain boundaries at which the cyclic conditions for wind and temperature are applied

The Smagorinsky eddy-viscosity model is used to parametrize small eddies that cannot be explicitly resolved by the LES model (Cui et al. 2004). In the tensor notation the Smagorinsky model is:

$$\tau_{ij} - \frac{1}{3}\delta_{ij}\tau_{kk} = 2K_{\mathrm{m}}S_{ij}, \tag{3}$$

$$S_{ij} = \frac{1}{2}\left(\frac{\partial u_i}{\partial x_j} + \frac{\partial u_j}{\partial x_i}\right), \tag{4}$$

$$K_{\mathrm{m}} = l^2\sqrt{2S_{ij}S_{ij}}, \tag{5}$$

where the indices i or j refers to the coordinates i, $j = 1, 2, 3$ (x, y, z, respectively), τ_{ij} is the subgrid-scale stress tensor, K_{m} is the subgrid-scale turbulent viscosity, δ_{ij} is the Kronecker symbol, S_{ij} is the rate-of-strain tensor for the resolved scale flow, and l is the subgrid-scale turbulent characteristic length scale given by

$$l = C_{\mathrm{S}}\left(\Delta x \Delta y \Delta z\right)^{1/3}, \tag{6}$$

where C_{S} is the Smagorinsky model parameter. Too large a value of C_{S} provides excessive dissipation but too small a value carries numerical errors. The optimal choice of C_{S} tested in Cui et al. (2004) is used: $C_{\mathrm{S}} = 0.08$ if $z/H < 0.9$, and $C_{\mathrm{S}} = 0.1$ if $z/H > 1.1$; if $0.9 \leq z/H \leq 1.1$, a linear interpolation between 0.08 and 0.1 is specified. For temperature, the same subgrid-scale model is adopted for the subgrid-scale eddy thermal diffusivity: $K_{\mathrm{h}} = 3.0K_{\mathrm{m}}$ (Stevens et al. 1999). This implies that the turbulent Prandtl number ($Pr_t = K_{\mathrm{m}}/K_{\mathrm{h}}$) is 0.33, which has been widely adopted for convective atmospheric flows (Stevens et al. 1999). This value of Pr_t is within the range suggested by Huang et al. (2008) for the convective boundary layer.

Table 1 Specification of the simulations

UWH case	ΔT_U (K)	ΔT_D (K)	DWH case	ΔT_U (K)	ΔT_D (K)	Ri_w
00	0	0				0
10	1	0	01	0	1	−0.14
30	3	0	03	0	3	−0.43
50	5	0	05	0	5	−0.70
70	7	0	07	0	7	−0.97
90	9	0	09	0	9	−1.27
A0	10	0	0A	0	10	−1.41
B0	11	0	0B	0	11	−1.55
C0	12	0	0C	0	12	−1.72
E0	14	0	0E	0	14	−2.01
F0	15	0	0F	0	15	−2.14

Here, 'UWH Case' means an upstream-wall-heated case, 'DWH Case' means a downstream-wall-heated case, ΔT_U and ΔT_D are the difference between the temperature at the upstream wall and the downstream wall, respectively, and the temperature of the boundary layer. Ri_w is the wall Richardson number defined by Eq. 10

The temperature at $t = 0$ is uniform everywhere ($T_\infty = 293$ K) and the LES model runs for 1800 s with no thermal effect on the flow. The turnover time of the primary circulation, t_c, in the canyon is of the order of $t_c = (W + H)/U_c$, where U_c is the velocity scale of mean wind in the canyon. In all cases of this study, $U_c \approx 0.2\,\mathrm{m\,s^{-1}}$; therefore the value of t_c is about 180 s. In other words, a period of 1800 s is equivalent to $10t_c$. At $t = t_1 = 1800$ s, a neutrally driven turbulent field reaches a quasi-equilibrium state. Starting from $t = t_1$, a higher temperature is specified on the given urban facets to mimic the real conditions under which the facets receive solar radiation, as illustrated in Fig. 1. The simulations run for another 1800 s up to $t = t_2 = 3600$ s when the flow reaches a quasi-equilibrium state that is demonstrated by the time series of the primary first- and second-moment quantities of the flow. Finally, the simulations continue until $t_3 = 5400$ s. In the duration of $t \in [t_1, t_3]$, it will involve a development of a convective UBL (interpreted in time) above the canyon but its time scale is much larger than t_c and this justifies the 'quasi-equilibrium' state. The results presented herein are derived from the model fields for $t \in [t_2, t_3] \approx [20t_c, 30t_c]$.

Figure 1a represents the condition under which the solar radiation heats the building roof and the upstream wall. For simplicity, this is referred to as an upstream-wall-heated case, or an '*assisting case*' because the wind-generated primary vortex may be assisted by the thermal-generated updraft. In Fig. 1b, the building roof and the downstream wall are heated. This is referred to as a downstream-wall-heated case, or an '*opposing case*' because the wind-generated primary vortex may be opposed by the thermal-generated updraft. All cases in this study are described in Table 1. In the table, Cases 'd0' are the upstream-wall-heated cases illustrated by Fig. 1a and Cases '0d' are the downstream-wall-heated cases illustrated by Fig. 1b. The letter 'd' here represents $\Delta T = T_0 - T_\infty$, the temperature difference between the heated surface and the background air. As indicated in Table 1, 'd' is the value of ΔT for $\Delta T \leq 9$ K; for $\Delta T \geq 10$ K however, 'd' is a capitalized letter with a rule of one incremental letter corresponding to +1 K of ΔT. For example, 'A' is for $\Delta T = 10$ K, 'B' is for $\Delta T = 11$ K, etc. Case '00' is the neutral case in which all surface temperatures are equal to that of the air. It is assumed that the roof temperature is same as the temperature of the heated wall and the street-surface temperature is same as T_∞.

Several types of variables are derived statistically from the LES fields. The first type of the analyzed product is obtained by applying an operation over t and y, being therefore a function of (x, z). A second-moment resolved-scale quantity, denoted by $\langle\tilde{\varphi}\tilde{\psi}\rangle$, which is a function of (x, z), is defined based on the following averaging operator:

$$\langle\varphi\rangle_{t,y}(x,z) = \frac{1}{(t_3 - t_2)L_y}\int_{t_2}^{t_3}\int_{0}^{L_y}\varphi(t,x,y,z)\,\mathrm{d}y\mathrm{d}t. \tag{7}$$

In other words, $\langle\bullet\rangle_{t,y}$ denotes an average along the y-direction *and* over time. Such first-moment quantities include $\langle u\rangle_{t,y}$, $\langle w\rangle_{t,y}$, $\langle T\rangle_{t,y}$, the mean kinetic energy, $E(x,z) = \frac{1}{2}\left(\langle u\rangle_{t,y}^2 + \langle v\rangle_{t,y}^2 + \langle w\rangle_{t,y}^2\right)$, and the vertical advective fluxes (also termed as 'dispersive fluxes'), $F_{\mathrm{adv}}^{(\varphi)} = \langle w\rangle_{t,y}\langle\varphi\rangle_{t,y}$, specifically, $\langle w\rangle_{t,y}\langle T\rangle_{t,y}$. Following Eq. 7, $\tilde{\varphi}$ represents the resolved fluctuations of φ about $\langle\varphi\rangle_{t,y}$. Thus several second-moment quantities can be derived, and these may include: the mean resolved-scale TKE, $e(x,z) = \frac{1}{2}\left(\langle\tilde{u}^2\rangle_{t,y} + \langle\tilde{v}^2\rangle_{t,y} + \langle\tilde{w}^2\rangle_{t,y}\right)$; the mean turbulent intensities, $\sigma_{\tilde{\varphi}} = \sqrt{\langle\tilde{\varphi}^2\rangle_{t,y}}$, or specifically, $\sigma_{\tilde{T}}$, $\sigma_{\tilde{u}}$, $\sigma_{\tilde{v}}$ $\sigma_{\tilde{w}}$; the resolved-scale vertical turbulent fluxes, $F_{\mathrm{turb}}^{(\varphi)} = \langle\tilde{w}\tilde{\varphi}\rangle_{t,y}$, specifically $\langle\tilde{w}\tilde{T}\rangle_{t,y}$.

In order to show the integrated characteristics of the canopy layer, we average the above quantities inside the street canyon, i.e. in $\Omega_{\mathrm{canyon}} = \{(x,z): -0.5W \le x \le 0.5W, 0 \le z \le H\}$:

$$\overline{\varphi} = \frac{1}{WH}\int_{-0.5W}^{0.5W}\int_{0}^{H}\langle\varphi\rangle_{t,y}(x,z)\,\mathrm{d}x\mathrm{d}z. \tag{8}$$

Such defined *canyon-averaged* quantities include: $\overline{u}$, $\overline{w}$, $\overline{T}$, $\overline{E}$, and $\overline{e}$. For the fluxes, we focus on the roof level, $z = H$ and use the same symbol of 'bar' to define the averaged fluxes at the roof level:

$$\overline{F}^{(\varphi)} = \frac{1}{W}\int_{-0.5W}^{0.5W}F^{(\varphi)}(x,H)\,\mathrm{d}x. \tag{9}$$

The flux to be examined in this study is the sensible heat flux, $\overline{F}^{(T)}$.

The LES results shown here are derived from the whole domain (for all y) based on the averaging procedures mentioned above. The validity of the procedures is based on the ergodic property of all turbulent quantities along the y-direction. The advantage of using this method is being able to obtain reliable results for a relatively short simulation period, and it is particularly advantageous to adopt the method when the flow is not in complete equilibrium with the external conditions. As mentioned above, the cases in this study are in 'quasi-equilibrium' state; however, a duration of ten turnover times is sufficient.

We use the *wall Richardson number*, Ri_{w}, for any heated (or cooled) wall in the street canyon. The wall Richardson number is a dimensionless parameter that describes the ratio of thermal-generated kinetic energy (mainly in the updrafts near a heated wall) and wind-generated kinetic energy (mainly in the primary vortex), and is written as

$$Ri_{\mathrm{w}} = \frac{gH(T_{\mathrm{ref}} - T_0)}{T_{\mathrm{ref}}U_{\mathrm{ref}}^2}, \tag{10}$$

where T_{ref} is the mean temperature of the approaching air above the roof, and U_{ref} is the mean wind speed at height $2.5H$ above the roof level. The use of T_{ref} and U_{ref} is similar to that in the wind-tunnel experiments of Kovar-Panskus et al. (2002). In these experiments T_{ref} is the mean temperature of the approaching air above the roof and U_{ref} is the mean free-stream wind speed. In the LES, however, such free-stream flow does not exist. However, the wind profiles above the cavity of the experiments have been plotted in Fig. 2 of Kovar-Panskus et al. (2002) up to $1.8H$ above the roof level, and clearly showed that the wind speed reached about $0.95U_{\mathrm{ref}}$ at $z = 1.8H$. An extrapolation of the profiles to about $2.5H$ above the roof level would be a good approximation of U_{ref}. Therefore use of the mean wind speed at $2.5H$ above the roof as U_{ref} facilitates the comparisons in the next section. The wall Richardson number, Ri_{w}, and the canyon aspect ratio, H/W, form a set of controlling dimensionless parameters. It must be mentioned that the Froude number used by e.g. Kovar-Panskus et al. (2002) is in fact the reciprocal of $|Ri_{\mathrm{w}}|$:

$$Fr = |Ri_{\mathrm{w}}^{-1}|. \tag{11}$$

Thus their values of Fr will be converted into the corresponding values of Ri_{w} where needed.

This study will focus on the effects of the wall temperature on the flow characteristics in a street canyon by varying ΔT. Effectively these cases correspond to different values of the wall Richardson number and Table 1 shows the correspondence between ΔT and Ri_{w}. All the results will be presented against ΔT, which can be interpreted as, or translated into, a corresponding value of the wall Richardson number, Ri_{w}.

4 Results and Discussions

In this section, the following analyzed results are presented. First, the 2D fields of several quantities for Cases '90' and '09' will be shown as a demonstration of general characteristics of the flow, turbulence, and thermal structure: these are mean wind, mean turbulent intensities, mean TKE and its production rates, mean temperature, temperature fluctuation intensity, and the unsteadiness of the wind field. Second, the comparisons between the simulation results and wind-tunnel data are made in the form of mean 2D fields for wind and TKE. Third, the vertical profiles of mean TKE for five sets of cases ($\Delta T = 0, 3, 7, 11$, and 15 K) will be compared and discussed; then the influence of ΔT (or Ri_{w}) on the canyon-mean kinetic energy, the canyon-mean TKE, and the roof-level sensible heat flux is demonstrated. Finally, the results of the roof-level sensible heat flux and the canyon-mean temperature for $\kappa B_{\mathrm{H}}^{-1} = 5$ are compared with those for $\kappa B_{\mathrm{H}}^{-1} = 2$ as a demonstration of the importance of $\kappa B_{\mathrm{H}}^{-1}$.

4.1 Two-Dimensional Characteristics of Turbulent Flow

Figure 2 shows the mean flow patterns for Case '90' and Case '09' as an example. For the reason of technical simplicity of post-processing the model fields, the results above the roofs are not shown in all figures. For the upstream-wall-heated case (or assisting case, Case '90'), Fig. 2a demonstrates that the mean flow pattern is nearly symmetric about the centre; a small secondary vortex appears near the bottom-right corner of the canyon. The flow patterns of all other 'd0' cases (not shown) do not differ too much, except that the primary vortex intensity increases with the amount of wall heating. The figure shows that the influence of the primary vortex has been extended to above the roof level and will contribute significantly to the advective fluxes, which will be discussed in detail later. The results are consistent with those of previous CFD simulations (e.g. Sini et al. 1996).

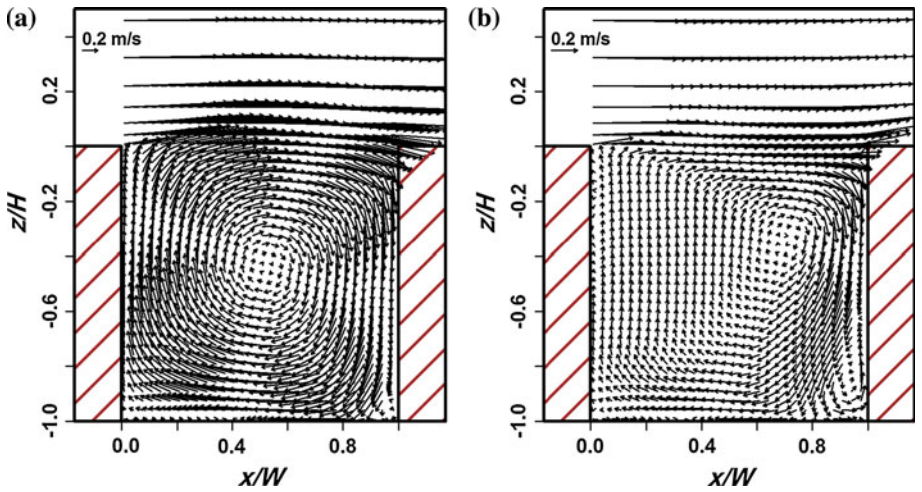

Fig. 2 Mean wind field $(\overline{u}, \overline{w})$ for: **a** Case '90'; **b** Case '09'

For the downstream-wall-heated (or opposing) case (Case '09') as shown in Fig. 2b, the centre of the mean primary vortex is shifted towards the upper-right direction. A secondary vortex near the bottom-right corner is much larger than that in Fig. 2a, suggesting that the secondary vortex is assisted by the downstream-wall heating. The intensity of the primary vortex is much lower than that of the assisting case shown in Fig. 2a. This is apparently attributed to the opposing effect from the thermal-driven updraft near the downstream wall heated by solar radiation. Furthermore, the influence of the primary vortex is confined below the roof level.

Figure 3a, c shows $\sigma_{\tilde{u}}/U_{\mathrm{ref}}$ and $\sigma_{\tilde{w}}/U_{\mathrm{ref}}$ for Case '90' (an assisting case), whereas Fig. 3b, d shows the two quantities for Case '09' (an opposing case). Because the boundary condition for temperature at the inlet/outlet is cyclic, the thermal energy (released from the heated wall) transferred above the roof level is retained within the domain. Consequently it contributes to the formation of a convective UBL above the roof level, resulting in high values of $\sigma_{\tilde{u}}/U_{\mathrm{ref}}$ and $\sigma_{\tilde{w}}/U_{\mathrm{ref}}$ above the roof level as shown in Fig. 3. The values of $\sigma_{\tilde{u}}/U_{\mathrm{ref}}$ are larger than those of $\sigma_{\tilde{w}}/U_{\mathrm{ref}}$ above the roof level and this finding is consistent with field observations (e.g. Rotach 1995). Figure 3 indicates that $\sigma_{\tilde{u}}$ is 'advected' into the canyon near the downstream wall and there is a small fraction of $\sigma_{\tilde{u}}$ generated above the road. The results also show that the turbulence is anisotropic (i.e. $\sigma_{\tilde{u}}$ and $\sigma_{\tilde{w}}$ at one point in space are different) in a large proportion of the area. There are differences between the results of an assisting case and an opposing case, but the most prominent difference is the value of $\sigma_{\tilde{w}}$ near the heated wall. For the assisting case, no significant $\sigma_{\tilde{w}}$ is found near the heated upstream wall as shown in Fig. 3c. This suggests that the thermally driven updrafts are in parallel with the mechanically driven primary vortex near the heated upstream wall, effectively reducing the wind shear and consequently reducing the production of turbulence there. For the opposing case, however, the highest fluctuating component is $\sigma_{\tilde{w}}$ near the heated downstream wall, as shown in Fig. 3d. This contributes to the high level of TKE near the heated wall seen in Fig. 4b.

Figure 4a, b shows the normalized mean resolved-scale TKE, $e(x,z)/U_{\mathrm{ref}}^2$, Fig. 4c, d shows the mechanical production rate of TKE (normalized by U_{ref}^3/H), and Fig. 4e, f shows the buoyant production rate of TKE (normalized by U_{ref}^3/H) for Cases '90' and Case '09'. As discussed above, the large TKE above the roof level in Fig. 4a, b is attributed to the formation

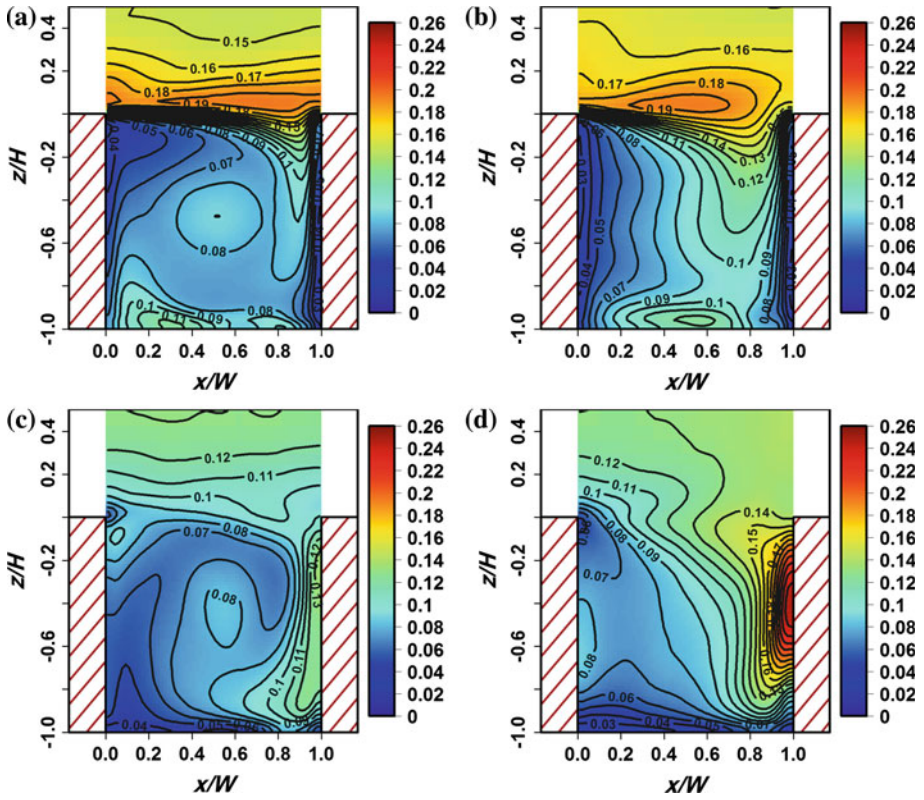

Fig. 3 Normalized mean turbulent intensities: **a** and **b** $\sigma_{\tilde{u}}/U_{\mathrm{ref}}$; **c** and **d** $\sigma_{\tilde{w}}/U_{\mathrm{ref}}$. The *left panels* are for Case '90' and the *right panels* are for Case '09'

of a convective UBL due to the thermal energy released from the heated wall. The mean TKE field for the opposing case, '09', as shown in Fig. 4b, has the highest level near the downstream wall. For the opposing case, the high TKE zone is much wider and the magnitude of TKE is much larger than that for the assisting case in Fig. 4a. Interestingly, the upstream-wall heating of the assisting case '90' contributes neither to the mechanical production (Fig. 4c) nor to the buoyant TKE production (Fig. 4e) near the heated wall. However it enhances the primary vortex (Fig. 2a) and contributes to the TKE production near the shear layer at the roof level as seen in Fig. 4c. The TKE mechanical production consists of the following terms (see Stull 1988): (i) the production by the wind shear: $-\langle\tilde{u}\tilde{w}\rangle_{t,y}\left(\frac{\partial\langle w\rangle_{t,y}}{\partial x}+\frac{\partial\langle u\rangle_{t,y}}{\partial z}\right)$; and (ii) the production by the normal deformation: $-\langle\tilde{u}^2\rangle_{t,y}\frac{\partial\langle u\rangle_{t,y}}{\partial x}-\langle\tilde{w}^2\rangle_{t,y}\frac{\partial\langle w\rangle_{t,y}}{\partial z}$. Term (i) contributes predominantly to the TKE production at the roof level where the shear deformation rate is high. In the places where the flow is deformed in the normal direction by the building or by the road, term (ii) becomes a non-negligible contribution. Term (ii) is positive if $\frac{\partial\langle u\rangle_{t,y}}{\partial x}<0$ or $\frac{\partial\langle w\rangle_{t,y}}{\partial z}<0$, i.e. if the mean flow is decelerated. For the assisting case this positive TKE production occurs in three locations along the path of the primary vortex in Fig. 4c: near the top of the downstream wall, near the bottom of the downstream wall, and near the left side of the road. For the opposing case this positive TKE production is only seen in two locations along the path of the primary vortex in Fig. 4d: near the top of the downstream wall and near the middle of the downstream wall. The higher location of the positive TKE production near

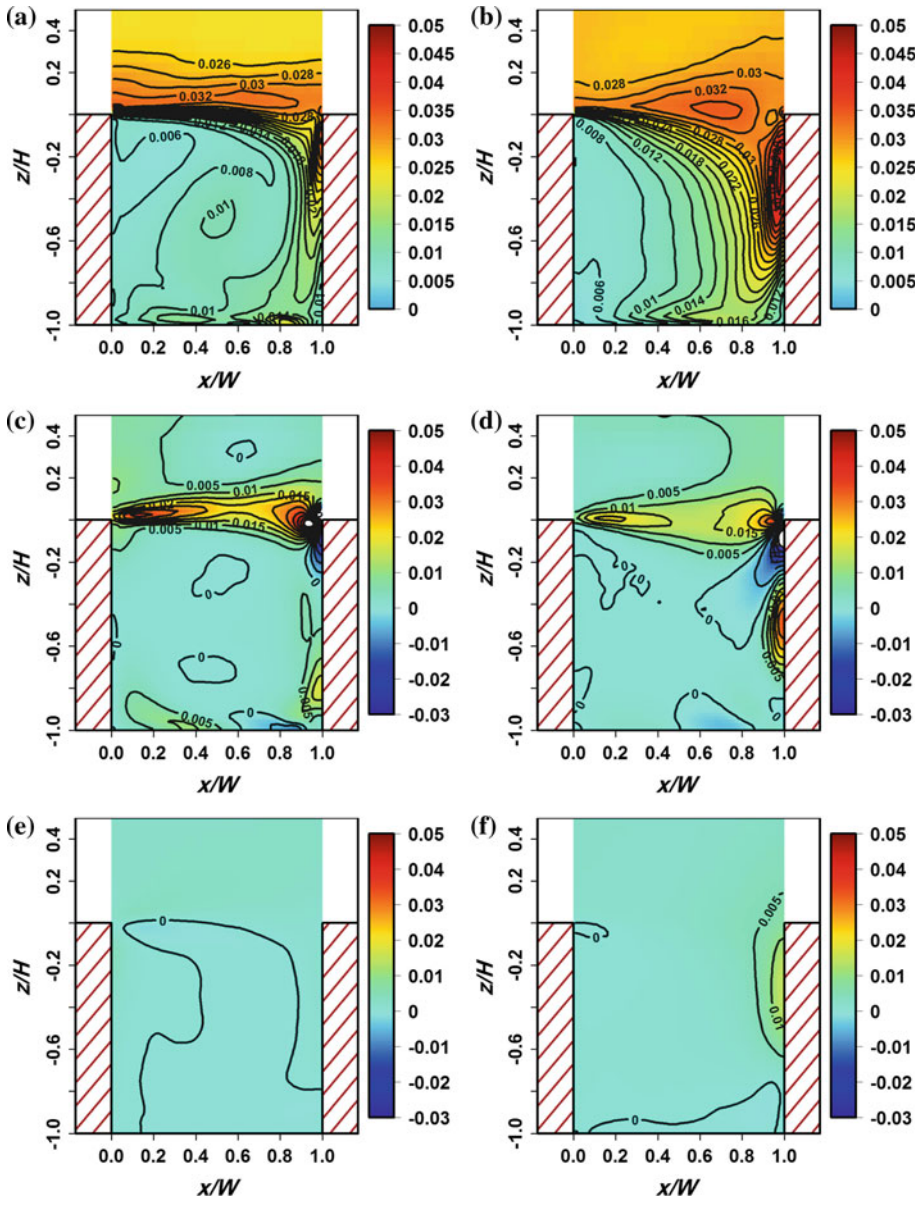

Fig. 4 **a** and **b** Mean TKE (normalized by U_{ref}^2); **c** and **d** mechanical production of TKE (normalized by U_{ref}^3/H); **e** and **f** buoyant production of TKE (normalized by U_{ref}^3/H). The *left panels* are for Case '90' and the *right panels* are for Case '09'

the downstream wall in Fig. 4d compared to that in Fig. 4c is attributed to the deceleration of the primary vortex by the large secondary vortex seen in Fig. 2b for the opposing case. Furthermore, term (ii) is negative if $\frac{\partial \langle u \rangle_{t,y}}{\partial x} > 0$ or $\frac{\partial \langle w \rangle_{t,y}}{\partial z} > 0$, i.e. if the mean flow is accelerated. As shown in Fig. 4c, d this negative TKE production occurs in two locations along the path of the primary vortex: near the top of the downstream wall, and near the right side of the

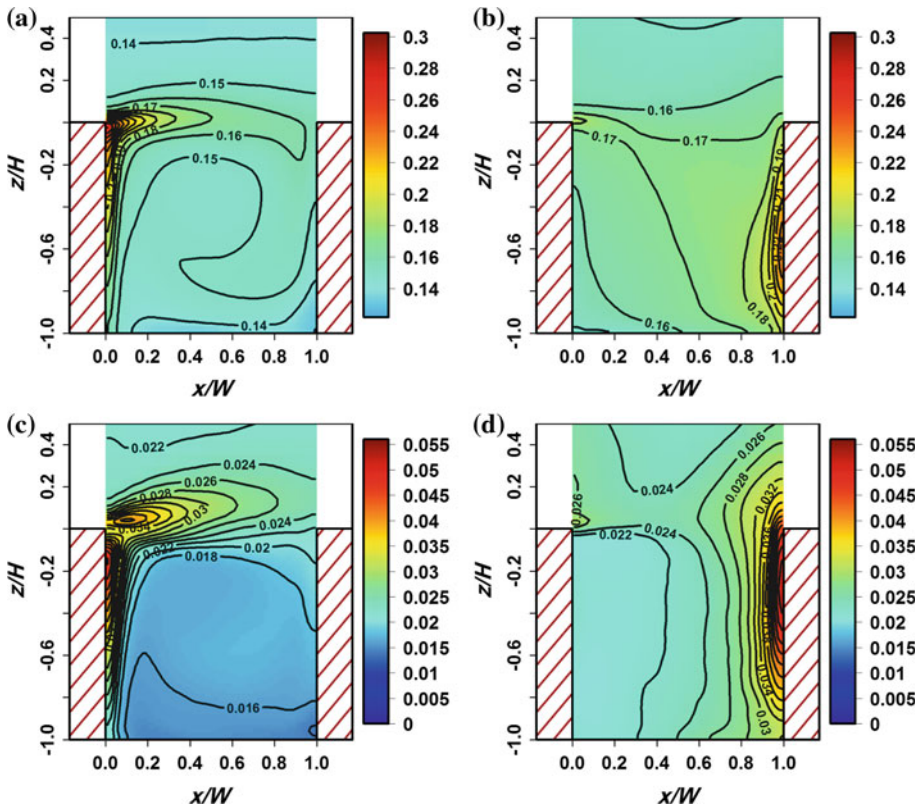

Fig. 5 **a** and **b** Normalized air temperature field increased by wall heating, $(\langle T\rangle_{t,y} - T_\infty)/\Delta T$; (c) and (d) normalized mean turbulent intensities of temperature, $\sigma_{\tilde{T}}/\Delta T$. The *left panels* are for Case '90' and the right panels are for Case '09'

road. Finally, Fig. 4e, f demonstrates that near the heated wall the buoyancy production term is negligible for the assisting case but considerable for the opposing case. Figure 4f shows that the high buoyancy production zone coincides with the location where the downward part of the wind-driven primary vortex confronts the upward thermal-driven updraft.

Figure 5 displays the results of $(\langle \mathrm{T}\rangle_{t,y} - T_\infty)/\Delta T$ and $\sigma_{\tilde{T}}/\Delta T$ for Case '90' in the left panels and Case '09' in the right panels. Because $\Delta T = T_0 - T_\infty$, the quantity $(\langle \mathrm{T}\rangle_{t,y} - T_\infty)/\Delta T$ represents the 'warming efficiency', or the fraction of canyon-air heating relative to the wall heating. Likewise the quantity $\sigma_{\tilde{T}}/\Delta T$ represents the relative magnitude of the turbulent intensity of temperature fluctuations. For the assisting case, Fig. 5a illustrates that the warming effect is confined within a narrow zone near the wall. In a large part of the canyon, the canyon air is warmed by approximately $0.15\Delta T$; or 15% of the wall heating is passed to the canyon air (warming efficiency of 15%). For the opposing case, however, the warming influences a larger part of the canyon due to turbulence. The canyon air is warmed approximately by $0.17\Delta T$, a higher warming efficiency than that of the assisting case. The results of $\sigma_{\tilde{T}}/\Delta T$ in Fig. 5c, d demonstrates that temperature fluctuations are large near the heated walls for both cases. The maximum value of $\sigma_{\tilde{T}}/\Delta T$ reaches about 0.055, implying that the maximum magnitude of temperature fluctuations is about 5.5% of ΔT. For the assisting case the fluctuations are advected above the roof level and little is entrained into the street canyon,

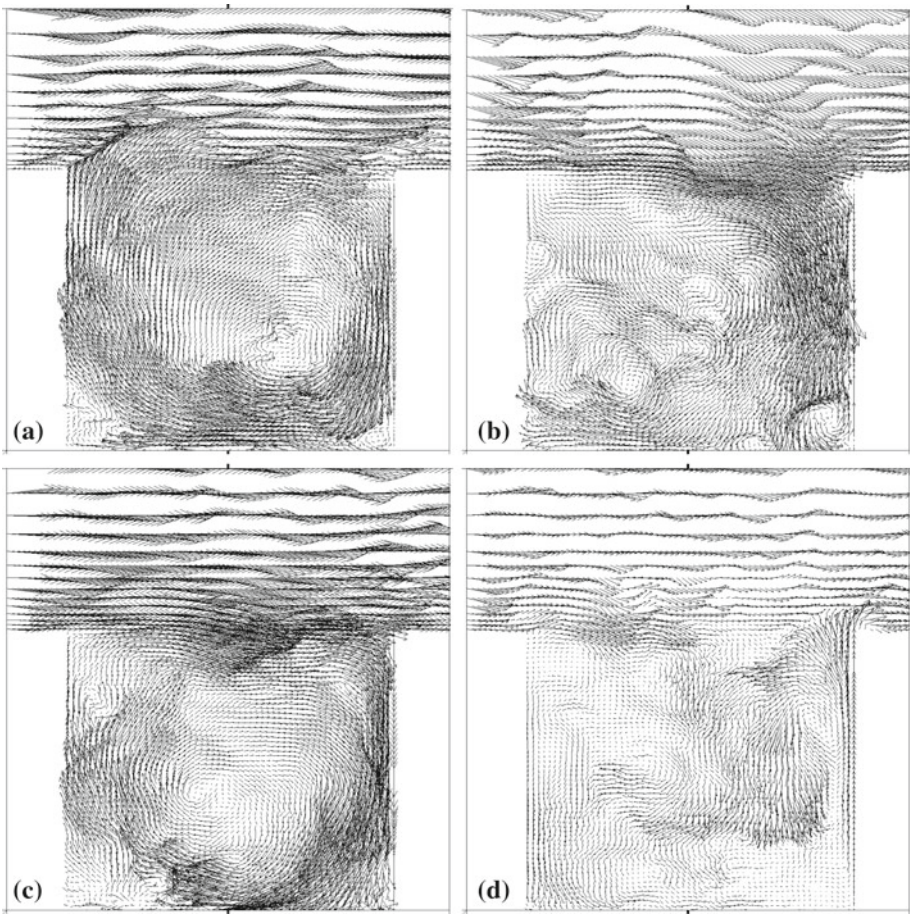

Fig. 6 Instantaneous wind fields (u, w) for two cases: **a** and **c** Case '90'; and **b** and **d** Case '09'

causing low values of $\sigma_{\tilde{T}}/\Delta T$ there (<0.016). For the opposing case, however, $\sigma_{\tilde{T}}/\Delta T$ is much higher inside the canyon (>0.022).

In order to demonstrate the unsteadiness of the flow, we present in Fig. 6 two snapshots of the wind field for each of Case '90' and Case '09'. For the assisting cases (Fig. 6a, c) the flow has a typical feature of an organized primary vortex with many embedded small eddies. At the roof level of the canyon, an ejection event (see Fig. 6a as an example) or a sweep event (see Fig. 6c as an example) is observed occasionally. The occurrence of the events is correlated to the flow structure above the canyon. For the opposing cases (Fig. 6b, d), however, the intensity of the primary vortex is weak and more medium-size eddies are found across the canyon. Figure 6b illustrates a flow pattern when a downdraft intrudes into the canyon, dominating the updraft near the heated wall. Such an event seems to be correlated with the phase of fluctuations above the canyon. The secondary vortex near the bottom-right corner of the canyon is reduced to a size much smaller than the averaged size shown in Fig. 2b. Figure 6d shows another extreme event for Case '09', namely, a penetrating updraft along the heated wall. This may happen when fluctuations above the canyon are weak and heat released by the wall accumulates. Two noticeable features for such an event are observed:

a narrow updraft zone and low occurring frequency. The width of the updraft is less than 1 m except for the region near the roof level. It is noted that the frequency of the event is so low that its contribution to the mean flow pattern shown in Fig. 2b is negligible. This may explain why such an updraft is rarely observed in field observations.

4.2 Comparison Between Simulation and Wind-Tunnel Experiment

In order to demonstrate the validity of the LES methodology, we compare the results of this study with measurement. Due to the reasons discussed in Sect. 1, such measurements are scarce. The wind-tunnel experiments of Kovar-Panskus et al. (2002) had the closest settings to the present LES runs. In the wind-tunnel experiments, the boundary layer was simulated using vorticity generators and low density, flat plates as roughness elements. The boundary-layer height was 1 m and the roughness length of these elements was about one tenth of the boundary layer height (Kovar-Panskus et al. 2002). Before the comparisons are made, several issues are discussed here:

1. The wind-tunnel experiments were conducted for only one heated cavity whereas the LES cases are configured for repeated arrays of street canyons (this is the consequence of the cyclic boundary conditions for wind and temperature). In addition, the cyclic boundary conditions in the LES cases imply an advection of the turbulence and the thermals generated from the upwind building-arrays. This is however not the case for the wind-tunnel experiments.
2. The LES cases are designed for a realistic condition of solar radiation with a zenith angle of 45°; therefore the wall and the *roof* are heated, whereas in the wind-tunnel experiments only the wall is heated. Combined with point 1 above, we expect more convectively generated turbulence above the roof level for the LES cases in comparison with the wind-tunnel experiments.
3. Kovar-Panskus et al. (2002) only presented the averaged 2D fields of the wind-tunnel results, and in addition they only conducted the downstream-wall-heated (opposing) cases. Therefore the comparisons shown here are restricted to these results.
4. A quantitative comparison between the wind-tunnel experiments and the LES cases relies on the justification of the Reynolds number (Re). For the wind-tunnel experiments $Re \sim 10^4$ whereas for the LES cases $Re \sim 10^6$. It is assumed herein that the results are independent of Reynolds number for this range of Re.
5. The definition of reference velocity may also be problematic due to the different settings between the wind-tunnel experiment and the LES. It is not possible to unify the definition of U_{ref} for both LES and wind-tunnel experiment. In the following LES results, the mean wind speed at $2.5H$ above the roof level is used for U_{ref}.
6. Since the wall surfaces of the wind-tunnel experiment are smooth, the LES results with $\kappa B_{\mathrm{H}}^{-1} = 2$ (representing a smoother wall surface) are chosen for the comparisons in Sect. 4.2.

Figure 7a displays the mean wind field of the LES case with $Ri_{\mathrm{w}} = -0.97$, while Fig. 7b shows the mean wind fields constructed from the profiles at five locations of the wind-tunnel experiment of Kovar-Panskus et al. (2002) for the case with $Ri_{\mathrm{w}} = -0.85$. Several features are seen in Fig. 7: (i) both have low wind speeds in the left part of the canyon; (ii) both have large wind speeds near the downstream wall; (iii) no updrafts are found near the top of the heated wall for both case; and (iv) at $x/W = 0.9$ in Fig. 7b, there exists a sector where air flows away from the wall. In fact, the combination of (i) and (ii) of the LES field should result in a shift of the primary vortex to the right constrained by the conservation of mass, as seen

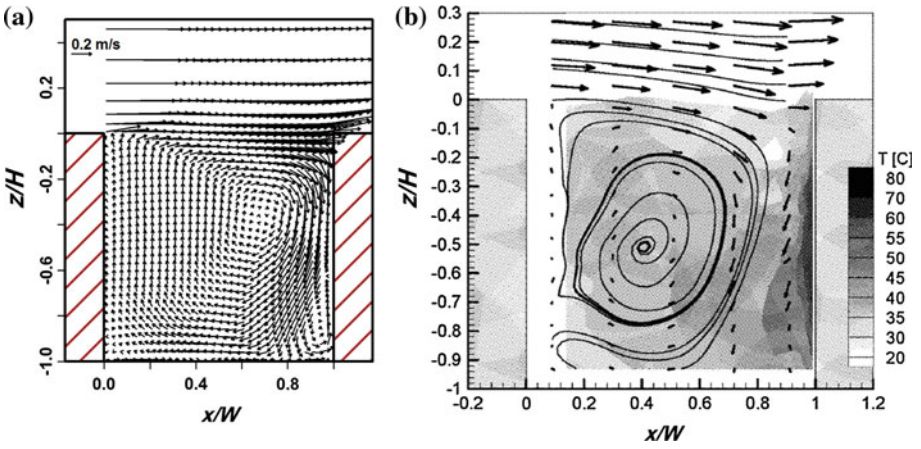

Fig. 7 **a** Mean wind field ($\overline{u}$, $\overline{w}$) for Case '07' with $Ri_{\mathrm{w}} = -0.97$; **b** Fig. 8 of Kovar-Panskus et al. (2002). Projected mean velocity vectors, streamlines, and mean temperature for the case with $Ri_{\mathrm{w}} = -0.85$

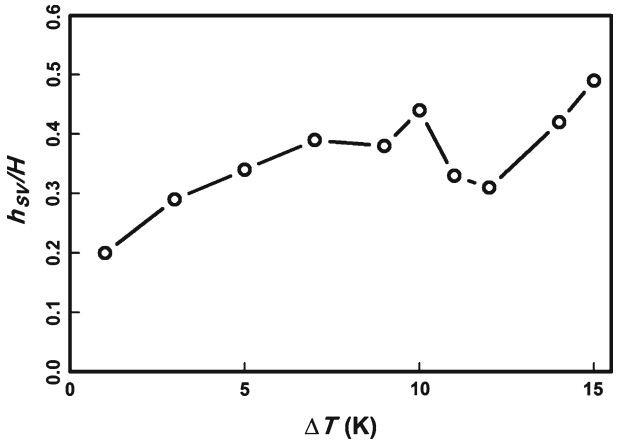

Fig. 8 Normalized height of the secondary vortex near the lower downstream wall as a function of ΔT for the opposing cases

in the LES results in Fig. 7a. However the sketched primary vortex in Fig. 7b is shifted to the left in the wind-tunnel result. Following the conservation of mass, this flow pattern should only be sustained by either a non-detected significant updraft very close to the wall or a mass divergence along the canyon axis. These were not discussed by Kovar-Panskus et al. (2002). With a careful look at the wind vectors near the lower-right corner of the canyon near the heated wall in Fig. 7b, we note that the two lowest vectors are towards the wall. In fact the turning of the wind vectors near the corner is more obvious for the other two wind-tunnel cases with higher level of wall heating (see Figs. 9 and 10 in Kovar-Panskus et al. 2002). Together with (iv) above, this indicates the existence of a secondary vortex but the updraft sector of the secondary vortex near the wall is too thin to be detected by the wind-tunnel experiment. Because of the secondary vortex there should be a stagnant point at which the vertical mean wind near the wall is zero. Here we define it as the height of the secondary vortex, h_{SV}. The LES results of all '0d' cases (Fig. 8) show that h_{SV} increases with ΔT (or equivalently $|Ri_{\mathrm{w}}|$) when ΔT is small, followed by a decrease and then an increase again.

The mechanism causing the oscillation is not clear and is worth investigating in the future. It is noted that none of the mean flow patterns displays an open updraft near the heated wall.

Using the renormalized-group k-ε turbulence model (the RANS methodology), Xie et al. (2007) derived the flow fields under the influence of the heated downstream wall with $Ri_{\mathrm{w}} = -0.49$, -0.85, and -1.34 (the figures are not displayed here). Their results showed that the centre of the primary vortex is elevated vertically but not significantly shifted horizontally. The secondary vortex near the downstream wall derived from the RANS model is much larger than that from the wind-tunnel experiment of Kovar-Panskus et al. (2002) and this applies to all three cases ($Ri_{\mathrm{w}} = -0.49$, -0.85, and -1.34) of Xie et al. (2007). As discussed in Sect. 1, the existence of such a persistent thick layer of updraft near the heated downstream wall is not supported by field observations either. The mean flow patterns derived from the present LES model with $Ri_{\mathrm{w}} = -0.43$, -0.97, and -1.41 all have a small secondary vortex (not shown here). This may be attributed to the LES's capability of resolving unsteady flow features. For example the analysis associated with Fig. 6 reveals that the LES model captures an unsteady penetrating narrow updraft zone that only occurs occasionally along the heated wall. The frequency of the event is so low that its contribution to the mean flow pattern shown in Fig. 7a is negligible. Such an unsteady penetrating narrow updraft cannot be represented by a RANS model, and is certainly worthy of further investigations.

Figure 9 presents the comparison of the normalized TKE fields between the wind-tunnel experiment and the LES. The five dotted lines in Fig. 9b, d indicates the locations where the wind-tunnel measurements were taken. Because all results in Fig. 9 are normalized by U_{ref}^2, a direct comparison between wind-tunnel experiment and LES can be made. Firstly, as discussed in point 2 above, a high TKE region above the roof level is seen in the LES fields, resulting in greater TKE inside the whole canyon. For the low heating case ($Ri_{\mathrm{w}} \approx -0.49$), the general pattern and the magnitude of TKE inside the canyon agree fairly well between the wind-tunnel experiment and the LES field (Fig. 9a, b). For the high heating case ($Ri_{\mathrm{w}} = -1.4$), the TKE of the LES is in general greater than that of the wind-tunnel experiment in a large proportion of the area inside the canyon (Fig. 9c, d). This is again attributed to the transfer of the high TKE above ($\approx$0.04) into the canyon. The highest TKE level near the heated wall is located around $0.7H$ above the ground for both wind-tunnel experiment and LES. It is worth noting that in comparison with the wind-tunnel experiments, the high TKE zone near the top of the heated wall simulated by the LES is thinner and its magnitude is weaker.

4.3 Effect of Wall Heating on TKE

Figure 10 presents the mean vertical profiles of the resolved-scale TKE at five selected locations, $x/W = 0.1$, 0.3, 0.5, 0.7, and 0.9 (for n =1, 2, 3, 4, and 5, respectively), for several selected heating cases. These case are '30', '70', 'B0', and 'F0' (Fig. 10 (UWH-n)), and the opposing cases, '03', '07', '0B', and '0F' (Fig. 10 (DWH-n)). The neutral case, '00', is also shown together with the four wall-heated cases of $\Delta T = 3$, 7, 11, and 15 K. The figures only display the bottom portion of the convective UBL. The results show that the TKE above the roof level has little dependence on the location, and in general, the TKE increases with wall heating both inside and outside of the canyon. The TKE is enhanced near the shear layer immediately above the canyon. A remarkable contrast between the assisting cases and the opposing cases is seen in the TKE profiles near the downstream wall, where the TKE enhancement by the wall heating is the most obvious characteristic of the opposing cases. This is consistent with the field observations of Offerle et al. (2007).

Figure 11 illustrates the effects of the wall heating on the mean kinetic energy ($\overline{E}$) and the resolved-scale TKE averaged inside the street canyon ($\overline{e}$). First, the partition between $\overline{E}$ and

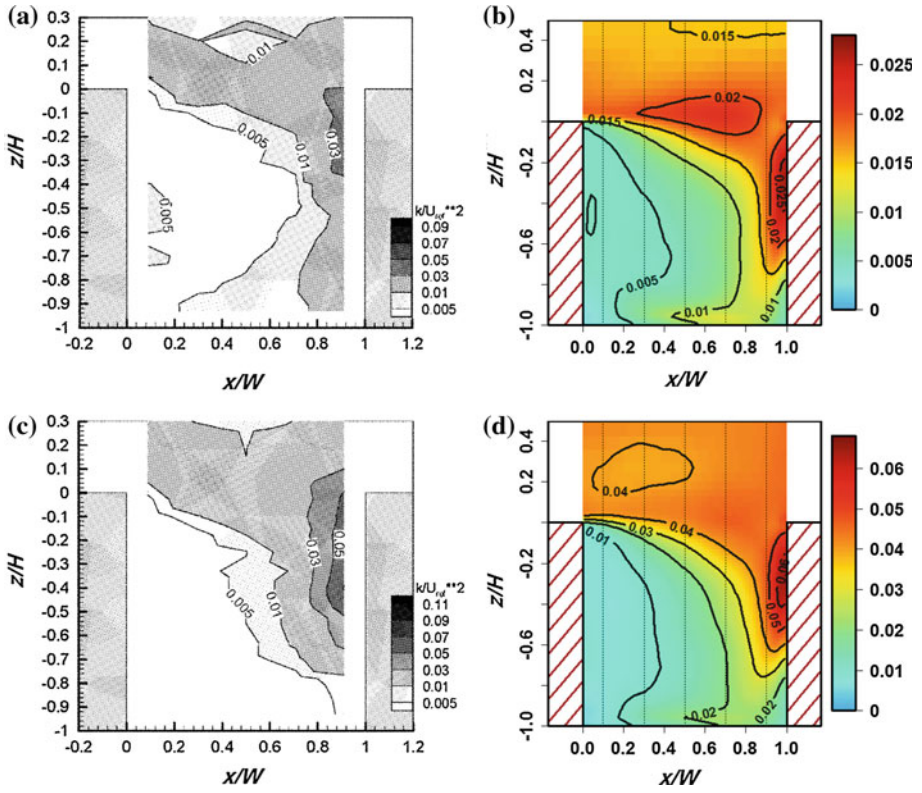

Fig. 9 Comparison of TKE fields between the wind-tunnel experiments (WTE) of Kovar-Panskus et al. (2002) and the present LES results. **a** WTE for $Ri_{\mathrm{w}} = -0.49$; **b** LES for $Ri_{\mathrm{w}} = -0.43$; **c** WTE for $Ri_{\mathrm{w}} = -1.37$; **d** LES for $Ri_{\mathrm{w}} = -1.41$. The five dotted lines in **b** and **d** indicate the locations at which the wind-tunnel measurements in **a** and **c** were taken

$\overline{e}$ is dramatically different between the assisting and the opposing groups: $\overline{E}$ dominates for the assisting group whereas $\overline{e}$ dominates for the opposing group. The contrast of $\overline{E}$ between the assisting and opposing groups suggests that the intensity of the primary vortex (indicated by $\overline{E}$) is increased by the upstream-wall heating but inhibited by the downstream-wall heating. It is interesting to see that for the opposing cases, the dependence of $\overline{E}$ on ΔT is quite complex: it decreases for $\Delta T < 3$ K, and it is nearly constant until $\Delta T \approx 10$ K after which $\overline{E}$ increases with ΔT and decreases again. The pattern of this variation with ΔT seems to be correlated to the height of the secondary vortex shown in Fig. 8. This behaviour indicates the alternative dominance by two driving mechanisms: the background flow and the wall heating. For both assisting and opposing cases, the TKE increases with ΔT in a linear manner. The TKE for the opposing cases is much larger than that for the assisting cases, suggesting that the interaction between the wind-driven primary vortex and the thermal-driven updrafts near the upper downstream wall serves as an efficient mechanism of generating TKE. In Fig. 11b, we can see that the total kinetic energy inside the canyon ($\overline{K} = \overline{E} + \overline{e}$) is enhanced by the increase of ΔT. This indicates an enhanced transfer of kinetic energy from the UBL to the street canyon by the wall heating. For the assisting cases, the total kinetic energy is raised by about $0.36\overline{K}_{00}$ per K of ΔT. That is, for every 2.76 K of ΔT, there is an increase of $\overline{K}_{00}$ for the total kinetic energy. For the opposing cases, the elevation of $\overline{K}$ appears in a much

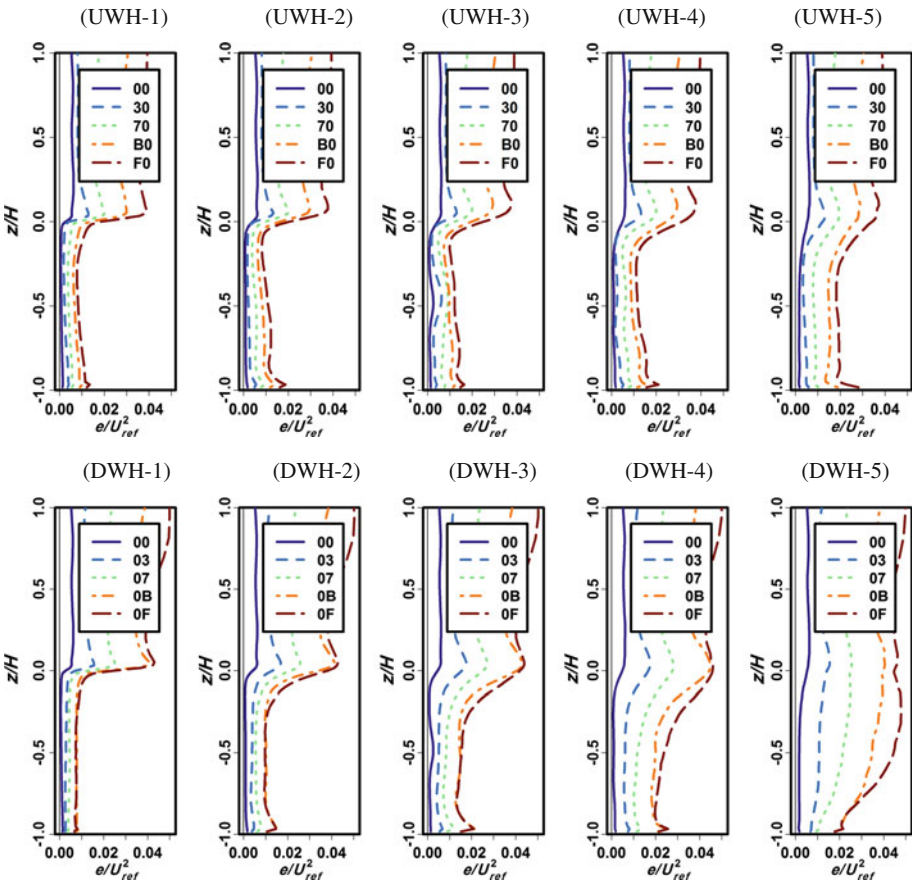

Fig. 10 Vertical profiles of $e\,(x, z)$ at $x/W = 0.1$, 0.3, 0.5, 0.7, and 0.9 (columns 1, 2, 3, 4 and 5, respectively) for the upstream-wall-heated (assisting) cases (*top row*) and the downstream-wall-heated (opposing) cases (*bottom row*)

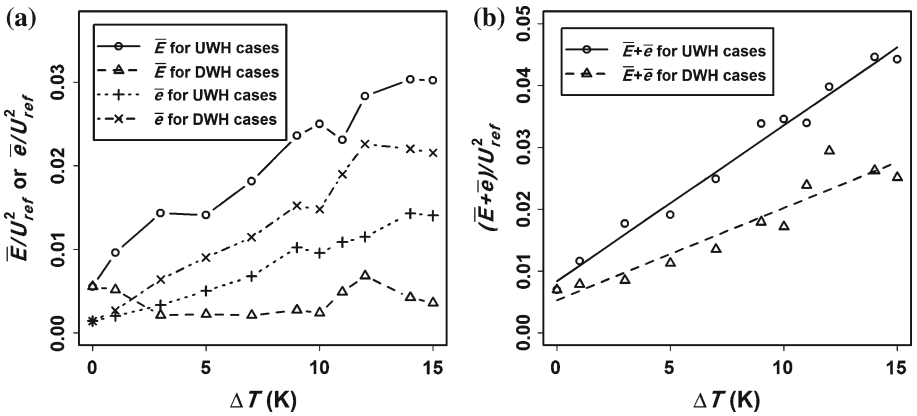

Fig. 11 **a** Mean kinetic energy, $\overline{E}$, and resolved-scale TKE, $\overline{e}$, inside the street canyon for all cases; **b** total kinetic energy, $\overline{K} = \overline{E} + \overline{e}$, with linear regression lines for the upstream-wall-heated (assisting) and downstream-wall-heated (opposing) cases

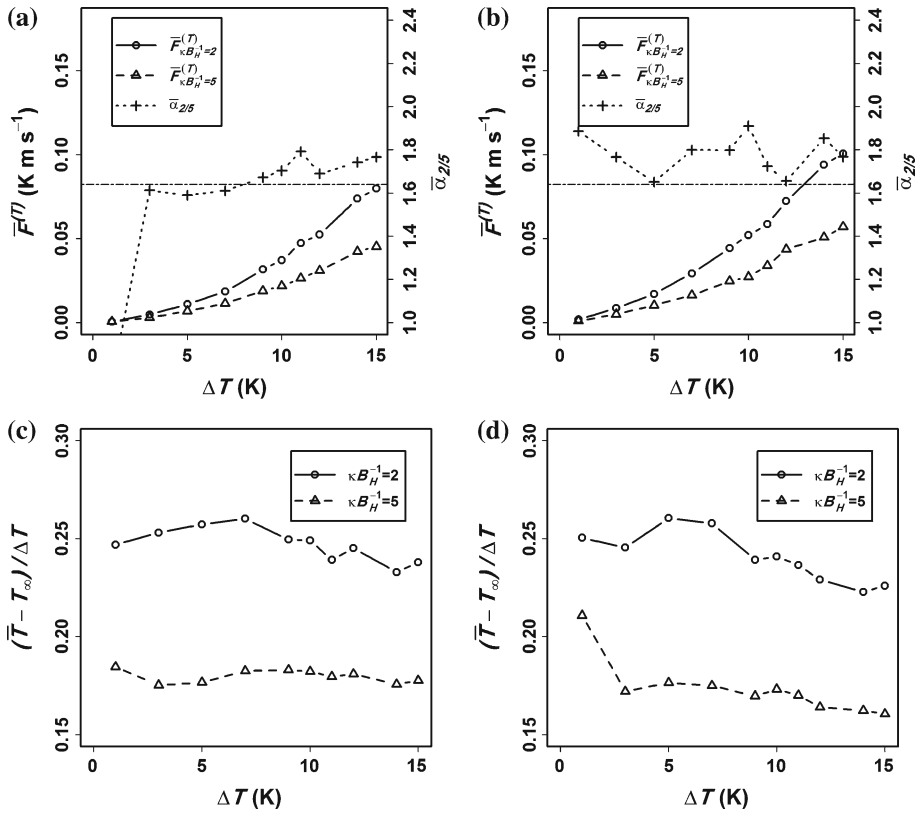

Fig. 12 **a** and **b** Mean total sensible heat flux at the roof level, $\overline{F}^{(T)}$, for $\kappa B_{\mathrm{H}}^{-1} = 2$ and $\kappa B_{\mathrm{H}}^{-1} = 5$ and the ratio of the two fluxes, $\overline{\alpha}_{2/5}$, as defined by Eq. 12; the *dash-dotted line* represents the value of $\alpha_{2/5,n} = 1.64$, the local ratio under the neutral limit as defined by Eq. 14. **c** and **d** normalized canyon-air temperature increased by wall heating, $(\overline{T} - T_\infty)/\Delta T$. The *left panels* are for the assisting group and the *right panels* are for the opposing group

smaller scale of about $0.21\overline{K}_{00}$ per K of ΔT. In other words, for every 4.67 K of ΔT, there is an increase of $\overline{K}_{00}$ for the total kinetic energy.

4.4 Effect of $\kappa B_{\mathrm{H}}^{-1}$ on the Sensible Heat Flux and Air Temperature

Finally we demonstrate the effect of the value of $\kappa B_{\mathrm{H}}^{-1}$ on the sensible heat flux at roof level ($\overline{F}^{(T)}$, as defined in Eq. 9) and the temperature in the canyon ($\overline{T}$, as defined in Eq. 8). Two values of $\kappa B_{\mathrm{H}}^{-1}$ are chosen: $\kappa B_{\mathrm{H}}^{-1} = 5$ represents a rougher surface and $\kappa B_{\mathrm{H}}^{-1} = 2$ represents a smoother surface. Figure 12 demonstrates that, for both assisting and opposing groups, the value of $\kappa B_{\mathrm{H}}^{-1}$ has a significant effect on the sensible heat flux: a smaller $\kappa B_{\mathrm{H}}^{-1}$ causes an enhancement of total sensible heat flux. Figure 12a, b also displays the ratios of the two total sensible heat fluxes:

$$\overline{\alpha}_{2/5} = \frac{\overline{F}^{(T)}_{\kappa B_{\mathrm{H}}^{-1}=2}}{\overline{F}^{(T)}_{\kappa B_{\mathrm{H}}^{-1}=5}} = \frac{\overline{F}^{(T)}_2}{\overline{F}^{(T)}_5} \tag{12}$$

where the subscripts, "2"and "5", denote the cases for $\kappa B_{\mathrm{H}}^{-1} = 2$ and $\kappa B_{\mathrm{H}}^{-1} = 5$, respectively. For the majority of the cases in both assisting and opposing groups, the values of $\overline{\alpha}_{2/5}$ are in the range of 1.6 to 1.9; the average value for the assisting group is 1.68 (excluding Case '10') and that for the opposing group is 1.78. As mentioned in Sect. 2, the value of $z_{0\mathrm{T}}$ in the wall function has a strong influence on the sensible heat flux at roof level. This influence is through the wall function, Eq. 1, which specifies the local sensible heat flux at the wall surface, $F_0^{(T)}$. When the turbulent flow is in dynamical quasi-equilibrium, the average of $F_0^{(T)}$ over the heated facet should be equal to $\overline{F}^{(T)}$, the flux at the roof level. Therefore $\overline{\alpha}_{2/5}$ is related to $\alpha_{2/5}$, which is the ratio of two wall fluxes ($F_0^{(T)}$ for $\kappa B_{\mathrm{H}}^{-1} = 2$ and $\kappa B_{\mathrm{H}}^{-1} = 5$). Furthermore, we have the following relationships for $\alpha_{2/5}$:

$$\alpha_{2/5} = \frac{F_{0,2}^{(T)}}{F_{0,5}^{(T)}} = \left(\frac{\ln\left(z_1/z_{0\mathrm{T},5}\right)}{\ln\left(z_1/z_{0\mathrm{T},2}\right)}\right) \cdot \frac{G_{T,2}|V_{1,2}|\Delta T_{1\text{-}0,2}}{G_{T,5}|V_{1,5}|\Delta T_{1\text{-}0,5}} \approx \frac{\ln\left(z_1/z_{0\mathrm{T},5}\right)\left(G_{T,2}\right)}{\ln\left(z_1/z_{0\mathrm{T},2}\right)\left(G_{T,5}\right)} = \frac{C_{T,2}}{C_{T,5}}. \quad (13)$$

The approximation in Eq. 13 is made based on an assumption that $V_1$and T_1 are the same for the two scenarios. Thus Eq. 13 shows that $\alpha_{2/5}$ can be approximated by the ratio of the two heat exchange coefficients, and under the neutral limit ($G_{\mathrm{T}} \to 1$), Eq. 13 yields

$$\alpha_{2/5} \approx \alpha_{2/5,n} = \frac{\ln\left(z_1/z_{0\mathrm{T},5}\right)}{\ln\left(z_1/z_{0\mathrm{T},2}\right)} = \frac{\ln\left(z_1/z_0\right) + \ln\left(z_0/z_{0\mathrm{T},5}\right)}{\ln\left(z_1/z_0\right) + \ln\left(z_0/z_{0\mathrm{T},2}\right)} = \frac{\ln\left(z_1/z_0\right) + 5}{\ln\left(z_1/z_0\right) + 2}, \quad (14)$$

where $\alpha_{2/5,n}$ is the ratio $\alpha_{2/5}$ under the neutral limit and $\ln\left(z_0/z_{0\mathrm{T}}\right) = \kappa B_{\mathrm{H}}^{-1}$. In the present study, $z_1 = 0.15$ m and $z_0 = 0.01$ m; therefore $\alpha_{2/5,n} \approx 1.64$. By plotting this value as the dash-dotted line in Fig. 12a, b, we find that $\overline{\alpha}_{2/5} \approx_{2/5,n}$, indicating that the ratio of two surface fluxes $F_{0,2}^{(T)}/F_{0,5}^{(T)}$ under the neutral limit is a good representation of the ratio of two roof-level fluxes $\overline{F}_2^{(T)}/\overline{F}_5^{(T)}$. It is therefore concluded that the near-facet process, which is parametrized by $\kappa B_{\mathrm{H}}^{-1}$ (or equivalently, $z_{0\mathrm{T}}$), is the primary factor in affecting the sensible heat flux, and that other processes such as in-canyon mixing and roof-level exchange are secondary.

Figure 12 also suggests that for the assisting group, the averaged $\overline{\alpha}_{2/5}$ of 1.68 (excluding Case '10') is only slightly higher than $\alpha_{2/5,n} = 1.64$. Figure 12a illustrates that $\overline{\alpha}_{2/5}$ is smaller than $\alpha_{2/5,n}$ when the wall heating is not strong ($\Delta T < 7$ K) and it becomes larger than $\alpha_{2/5,n}$ when the wall heating is strong ($\Delta T > 7$ K). For the opposing group, however, Fig. 12b illustrates that the average of $\overline{\alpha}_{2/5}$ is about 1.78, larger than $\alpha_{2/5,n} = 1.64$. The explanations are given as follows: the change of the $\kappa B_{\mathrm{H}}^{-1}$ value from 5 to 2 raises the sensible heat flux (Fig. 12a, b) and thus enhances the updrafts near the downstream wall. Consequently this weakens the mean primary vortex but enhances the turbulent fluctuations ($\tilde{w}$) near the heated wall (as illustrated in Fig. 3d). As a result, the magnitude of the local instantaneous tangential velocity, $|V_1|$ in Eq. 13, increases. It is noted that in the LES, the wall function Eq. 1 is applied to the instantaneous velocity, $|V_1|$, and therefore it enhances the sensible heat flux. This feedback process results in a higher value of $\overline{\alpha}_{2/5}$ than $\alpha_{2/5,n}$ (the neutral-limit value).

Figure 12c, d presents $(\overline{T} - T_\infty)/\Delta T$, the elevated canyon-air temperature (averaged inside the canyon) by wall heating normalized by ΔT. In general, by changing $\kappa B_{\mathrm{H}}^{-1}$ from 5 to 2, the elevated temperature $\overline{T} - T_\infty$ is significantly enhanced for both assisting and opposing groups. The quantity $(T - T_\infty)/\Delta T$ can be interpreted in the framework of Ohm's law analogy based on a one-box model. To adopt the analogy, the street canyon is assumed to be a well-mixed box subject to the heat transfer from an urban facet and to the boundary layer. For this purpose two resistances are introduced: the resistance between an *urban facet* and the *canyon air* ($r_{0C}^{(T)}$) and the resistance between the *canyon air* and the *UBL* ($r_{C\infty}^{(T)}$).

The sum of $r_{0C}^{(T)}$ and $r_{C\infty}^{(T)}$ is the resistance between an *urban facet* and the *UBL* ($r_{0\infty}^{(T)}$), i.e. $r_{0\infty}^{(T)} = r_{0C}^{(T)} + r_{C\infty}^{(T)}$. For short, $r_{0C}^{(T)}$ is also called the facet-canyon resistance, $r_{C\infty}^{(T)}$ is the canyon-UBL resistance, and $r_{0\infty}^{(T)}$ is the facet-UBL resistance or the total resistance. The following relationships then follow directly from Ohm's law:

$$\overline{F}^{(T)} = \frac{\Delta T}{r_{0\infty}^{(T)}} = \frac{\overline{T} - T_\infty}{r_{C\infty}^{(T)}} = \frac{T_0 - \overline{T}}{r_{0C}^{(T)}}, \tag{15}$$

which yields $(\overline{T} - T_\infty)/\Delta T = r_{C\infty}^{(T)}/r_{0\infty}^{(T)}$. Here $(\overline{T} - T_\infty)/\Delta T$ represents the efficiency of the canyon air warmed by the wall heating, and $r_{C\infty}^{(T)}/r_{0\infty}^{(T)}$ represents the fraction of the canyon-UBL resistance to the facet-UBL resistance. Figure 12c, d shows that for $\kappa B_{\mathrm{H}}^{-1} = 5$, the canyon air is heated by about 16–18% of ΔT, but for $\kappa B_{\mathrm{H}}^{-1} = 2$, it is heated up to 22–25% of ΔT. This indicates that a reduced $\kappa B_{\mathrm{H}}^{-1}$ (a smoother urban facet) causes a higher mean temperature. From the perspective of resistance, the canyon-UBL resistance of the group with $\kappa B_{\mathrm{H}}^{-1} = 5$ is approximately 16–18% of the total resistance, whilst the facet-canyon resistance is about 82–84% of the total resistance. In other words, a large proportion of the total resistance arises from the facet-canyon resistance. If $\kappa B_{\mathrm{H}}^{-1} = 2$ is used (a smoother urban facet), the facet-canyon resistance falls to 75–78% of the total resistance.

We thus conclude that the use of the appropriate value of parameter $\kappa B_{\mathrm{H}}^{-1}$ (or equivalently z_{0T} in Eq. 1) in the wall function is vital to a successful numerical simulation of street-canyon flows with any facet-air exchange processes of heat or any scalar. The value of $\kappa B_{\mathrm{H}}^{-1}$ should be carefully chosen for a given surface based on our previous knowledge. This study also raises an awareness of the demand for a better knowledge of the $\kappa B_{\mathrm{H}}^{-1}$ values for various urban surfaces.

5 Conclusions

We develop a LES model based on a numerical meteorological model for street-canyon airflow with heated building facets. The boundary condition for temperature is given as a constant value at the heated facets and the wall function adopted for temperature is based on a scheme for the atmospheric surface layer (Uno et al. 1995). The LES model is applied to a canyon with the aspect ratio of unity for two idealized heating scenarios: (1) the roof and the upstream wall are heated, and (2) the roof and the downstream wall are heated.

Comparisons of 2D mean wind and TKE fields are made against the wind-tunnel experiments of Kovar-Panskus et al. (2002). The differences and similarities in the settings (controlling parameters and conditions of simulations) between the wind-tunnel experiment and the LES are carefully considered and discussed. One major difference is that the LES cases represent a TKE-rich convective UBL above the roof level driven by the wall/roof heating whilst in the wind-tunnel experiments the upstream inflow is neutral. The comparisons demonstrate that the LES model is capable of reproducing major flow features and TKE field inside the canyon.

For the assisting cases (i.e. the upstream wall is heated), the following flow characteristics are found: (1) the mean flow pattern is nearly symmetric and the primary vortex extends to above the roof level; (2) the primary vortex is accelerated by the wall heating, contributing to the dominating kinetic energy in comparison to the canyon-averaged mean TKE, although the latter is also enhanced by the wall heating; (3) a negligible TKE production is found near the heated wall; and (4) the heat transfer out of the canyon is mainly through the primary vortex within a narrow zone near the heated wall. For the opposing cases (i.e. the downstream

wall is heated), the following flow characteristics are found: (1) the mean flow patterns are fairly asymmetric; (2) the primary vortex intensity is significantly suppressed by the downstream-wall heating, a secondary vortex is assisted by the downstream-wall heating, and its size does not always grow monotonically with the wall heating; (3) the interaction between the primary vortex and the thermally driven updrafts generates a significant amount of TKE and the canyon-averaged TKE is enhanced by the wall heating; this is consistent with the field observations of Offerle et al. (2007); and (4) an unsteady penetrating narrow updraft zone appears occasionally along the heated wall and this feature is consistent field observations. The unique result indicates the superior capability of LES.

The impact of the key parameter $\kappa B_{\mathrm{H}}^{-1}$ on the simulation results is investigated by examining the roof-level sensible heat flux and mean canyon-air temperature for two values of $\kappa B_{\mathrm{H}}^{-1}$, in which $\kappa B_{\mathrm{H}}^{-1} = 5$ represents a rougher surface and $\kappa B_{\mathrm{H}}^{-1} = 2$ represents a smoother surface. It is demonstrated that for both assisting and opposing groups, the effect of the $\kappa B_{\mathrm{H}}^{-1}$ value is significant. By using $\kappa B_{\mathrm{H}}^{-1} = 2$ instead of 5, the sensible heat flux is enhanced by 60–90% and the canyon-air temperature difference, $\overline{T} - T_{\infty}$, is enhanced by about 33–47%. The averaged enhancement of sensible heat flux is 68% for the assisting group and 78% for the opposing group. The averaged enhancement of $\overline{T} - T_{\infty}$ is 37% for the assisting group and 39% for the opposing group. Further analysis demonstrates that the enhancement of sensible heat flux under the neutral limit (due to the near-facet processes) is 64%. It is therefore concluded that the near-facet process, which is parametrized by $\kappa B_{\mathrm{H}}^{-1}$ (or equivalently, $z_{0\mathrm{T}}$), is the primary factor in affecting the sensible heat, flux and other processes such as in-canyon mixing and roof-level exchange are secondary. It is thus vital to choose an appropriate value of this parameter in a numerical simulation of street-canyon flows with any facet-air exchange processes of heat or any scalar. This study also raises an awareness of the demand for carefully designed laboratory or field experiments of quantifying the value of $\kappa B_{\mathrm{H}}^{-1}$ (or equivalently, $z_{0\mathrm{T}}$) for various urban surfaces as well as deriving more useful datasets of the opposing cases for model validation.

Acknowledgements The computations described herein were performed using the University of Birmingham's BlueBEAR HPC service, which was purchased through HEFCE SRIF-3 funds. See http://www.bear.bham.ac.uk for more details.

References

Baik JJ, Kim JJ (1999) A numerical study of flow and pollutant dispersion characteristics in urban street canyons. J Appl Meteorol 38:1576–1589

Barlow JF, Harman IN, Belcher SE (2004) Scalar fluxes from urban street canyons. Part I: laboratory simulation. Boundary-Layer Meteorol 113:369–385

Brutsaert W (1975) Theory for local evaporation (or heat-transfer) from rough and smooth surfaces at ground level. Water Resour Res 11:543–550

Brutsaert W (1982) Evaporation into the atmosphere. Reidel Publishing Company, London 299

Cai XM, Barlow JF, Belcher SE (2008) Dispersion and transfer of passive scalars in and above street canyons-Large-eddy simulations. Atmos Environ 42:5885–5895

Cotton WR, Pielke RA, Walko RL, Liston GE, Tremback CJ, Jiang H, McAnelly RL, Harrington JY, Nicholls ME, Carrio GG, McFadden JP (2003) RAMS 2001: current status and future directions. Meteorol Atmos Phys 82:5–29

Cui ZQ, Cai XM, Baker CJ (2004) Large-eddy simulation of turbulent flow in a street canyon. Q J Roy Meteorol Soc 130:1373–1394

Garratt JR (1992) The atmospheric boundary layer. Cambridge University Press, Cambridge 316

Grimmond CSB, Oke TR (1999) Heat storage in urban areas: local-scale observations and evaluation of a simple model. J Appl Meteorol 38:922–940

Huang HY, Stevens B, Margulis SA (2008) Application of dynamic subgrid-scale models for large-eddy simulation of the daytime convective boundary layer over heterogeneous surfaces. Boundary-Layer Meteorol 126:327–348
Idczak M, Mestayer P, Rosant JM, Sini JF, Violleau M (2007) Micrometeorological measurements in a street canyon during the joint ATREUS-PICADA experiment. Boundary-Layer Meteorol 124:25–41
Kawai T, Kanda M (2010) Urban energy balance obtained from the comprehensive outdoor scale model experiment. part ii: comparisons with field data using an improved energy partition. J Appl Meteorol Climatol 49:1360–1376
Kim JJ, Baik JJ (2004) A numerical study of the effects of ambient wind direction on flow and dispersion in urban street canyons using the RNG k-epsilon turbulence model. Atmos Environ 38:3039–3048
Kovar-Panskus A, Moulinneuf L, Savory E, Abdelqari A, Sini J-F, Rosant J-M, Robins A, Toy N (2002) A wind tunnel investigation of the influence of solar-induced wall-heating on the flow regime within a simulated urban street canyon. Water Air Soil Pollut 2:555–572
Li XX, Britter RE, Koh TY, Norford LK, Liu CH, Entekhabi D, Leung DYC (2010) Large-eddy simulation of flow and pollutant transport in urban street canyons with ground heating. Boundary-Layer Meteorol 137:187–204
Liu CH, Barth MC (2002) Large-eddy simulation of flow and scalar transport in a modelled street canyon. J Appl Meteorol 41:660–673
Liu CH, Barth MC, Leung DYC (2004) Large-eddy simulation of flow and pollutant transport in street canyons of different building-height-to-street-width ratios. J Appl Meteorol 43:1410–1424
Liu CH, Leung DYC, Barth MC (2005) On the prediction of air and pollutant exchange rates in street canyons of different aspect ratios using large-eddy simulation. Atmos Environ 39:1567–1574
Louis JF (1979) Parametric model of vertical eddy fluxes in the atmosphere. Boundary-Layer Meteorol 17:187–202
Louka P, Vachon G, Sini JF, Mestayer PG, Rosant JM (2002) Thermal effects on the airflow in a street canyon—Nantes '99 experimental results and model simulations. Water Air Soil Pollut 2:351–364
Nakamura Y, Oke TR (1988) Wind, temperature and stability conditions in an east west oriented urban canyon. Atmos Environ 22:2691–2700
Narita KI (2007) Experimental study of the transfer velocity for urban surfaces with a water evaporation method. Boundary-Layer Meteorol 122:293–320
Offerle B, Eliasson I, Grimmond CSB, Holmer B (2007) Surface heating in relation to air temperature, wind and turbulence in an urban street canyon. Boundary-Layer Meteorol 122:273–292
Oleson KW, Bonan GB, Feddema J, Vertenstein M, Grimmond CSB (2008) An urban parameterization for a global climate model. Part I: formulation and evaluation for two cities. J Appl Meteorol Climatol 47:1038–1060
Richards K, Schatzmann M, Leitl B (2006) Wind tunnel experiments modelling the thermal effects within the vicinity of a single block building with leeward wall heating. J Wind Eng Ind Aerodyn 94:621–636
Rotach MW (1995) Profiles of turbulence statistics in and above an urban street canyon. Atmos Environ 29:1473–1486
Salamanca F, Krpo A, Martilli A, Clappier A (2010) A new building energy model coupled with an urban canopy parameterization for urban climate simulations-part I. formulation, verification, and sensitivity analysis of the model. Theor Appl Climatol 99:331–344
Sini JF, Anquetin S, Mestayer PG (1996) Pollutant dispersion and thermal effects in urban street canyons. Atmos Environ 30:2659–2677
Solazzo E, Britter RE (2007) Transfer processes in a simulated urban street canyon. Boundary-Layer Meteorol 124:43–60
Stevens B, Moeng CH, Sullivan PP (1999) Large-eddy simulations of radiatively driven convection: sensitivities to the representation of small scales. J Atmos Sci 56:3963–3984
Stull RB (1988) An introduction to boundary layer meteorology. Kluwer Academic Publishers, Dordrecht 666
Uehara K, Murakami S, Oikawa S, Wakamatsu S (2000) Wind tunnel experiments on how thermal stratification affects flow in and above urban street canyons. Atmos Environ 34:1553–1562
Uno I, Cai XM, Steyn DG, Emori S (1995) A simple extension of the Louis method for rough surface layer modelling. Boundary-Layer Meteorol 76:395–409
Xie XM, Huang Z, Wang JS, Xie Z (2005) Thermal effects on vehicle emission dispersion in an urban street canyon. Transp Res D 10:197–212
Xie XM, Liu CH, Leung DYC, Leung MKH (2006) Characteristics of air exchange in a street canyon with ground heating. Atmos Environ 40:6396–6409
Xie XM, Liu CH, Leung DYC (2007) Impact of building facades and ground heating on wind flow and pollutant transport in street canyons. Atmos Environ 41:9030–9049